Application of Flux Diverters in High Temperature Superconducting Transformer Windings for AC Loss Reduction

X. Y. Fang, X. L. Wang, Y. M. Sun, W. Song, X. Pei, Z. N. Jiang, R. Badcock, N. J. Long and J. Fang

***Abstract*—Flux diverters (FDs) are used in High Temperature Superconducting (HTS) transformers for AC loss reduction and flux optimization. In this paper, a 2D axial symmetric superconducting winding model is proposed and two designs of flux diverters are applied to the windings. A homogenization approach is used to analyze the windings with large turn numbers. The key parameters including the number, width, height and the spatial positions of the FDs are adjusted for AC loss and magnetic flux analysis. The means of obtaining optimum designs of the FDs is provided and can be used to develop new winding designs with FDs, which contributes to better electromagnetic performance and higher efficiency of HTS transformers.**

***Index Terms*—HTS transformer, Concentric Windings, AC loss analysis, magnetic flux analysis**

I. Introduction

WORLDWIDE energy deficiency and greenhouse gas emissions inhibit economic growth and aggravate environmental problems. In recent years, green technologies are applied in many power applications for energy saving purposes. Superconductivity is one of the promising approaches for the power loss reduction [1]-[3]. The advantages of superconducting technologies include high efficiency, no risk of fire and environment friendliness [4], [5]. Furthermore, superconducting devices support high current with small mass and volume [6]. Operations in low temperature conditions avoid aging effects and guarantee longevity of these devices.

High temperature superconducting (HTS) transformers are among main applications of the superconducting devices [7]-[11]. They can be used in power and high speed railway systems with notable increase of efficiency and dynamics [12]. Windings wound by multi-turn HTS tapes are fundamental parts of these applications, which are comprised of primary and secondary windings for power conversion. It has been found that magnetic flux penetration is highly associated with the performance of 1G and 2G HTS windings [13]-[16]. The AC losses of windings introduced by radial magnetic field influence the efficiency and stability of cooling systems. One of the solutions is to apply high permeability flux diverters (FDs) to the ends of windings [17]-[25]. In [17], FDs were applied to the windings of a 6.5 MVA HTS transformer, which led to notable AC loss, radial magnetic field and penetration area reduction. In [18], the effects of FDs in a 6.6 MVA HTS transformer were analyzed. In [19], short circuit force reduction for HTS transformer windings was achieved by optimization design of FDs. They were also used for improving both DC and AC performances of HTS coils [20]. These results have shown the effectiveness of FDs. However, a comprehensive analysis of FDs is still necessary for reference of modeling highly efficient HTS windings.

In this paper, a 2D axial symmetric 1.65 MVA HTS transformer winding model is developed using COMSOL Multiphysics. The model is comprised of a pair of concentric windings, including a low voltage (LV) winding and a high voltage (HV) winding. Flux diverters are applied to the ends of windings. An in-depth research of the influence of the FDs on the windings is provided. The key parameters including the number, width, height and spatial positions of flux diverters are adjusted. The AC losses and magnetic flux densities are obtained for analysis. The results indicate that the key parameters are critical to the AC loss reduction.

The remainder of this paper is organized as follows. Section 2 introduces the structural designs of the windings with the FDs, and a homogenization approach to reduce the computation cost of the windings with large turn numbers. Means of evaluating the AC losses using the key parameters of the FDs are provided in Section 3. In Section 4, the magnetic flux distribution is used to analyze the mechanism of the FDs. Finally, Section 5 provides some concluding remarks of the paper.

II. Modeling of the HTS Windings with the Flux Diverters

A. Designs of the HTS Windings with the Flux Diverters

This work was supported by the Fundamental Research Funds for the Central Universities under Grant 2020YJS163. *(Corresponding author: Xilian Wang.)*

X. Y. Fang, X. L. Wang, Y. M. Sun and J. Fang are with School of Electrical Engineering, Beijing Jiaotong University, Beijing, 100044, China (e-mail: xlwang1@bjtu.edu.cn).

W. Song and X. Pei are with Department of Electronic and Electrical Engineering, The University of Bath, Bath, BA2 7AY, United Kindom.

Z. N. Jiang, R. Badcock and N. J. Long are with the Robinson Research Institute, Victoria University of Wellington, Lower Hutt, 5046, New Zealand.

Color versions of one or more of the figures in this paper are available online at http://ieeexplore.ieee.org.

Digital Object Identifier will be inserted here upon acceptance.

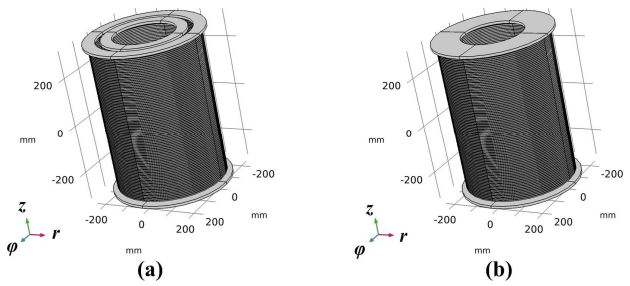

Fig. 1. Two designs of the FDs applied to the HTS windings.

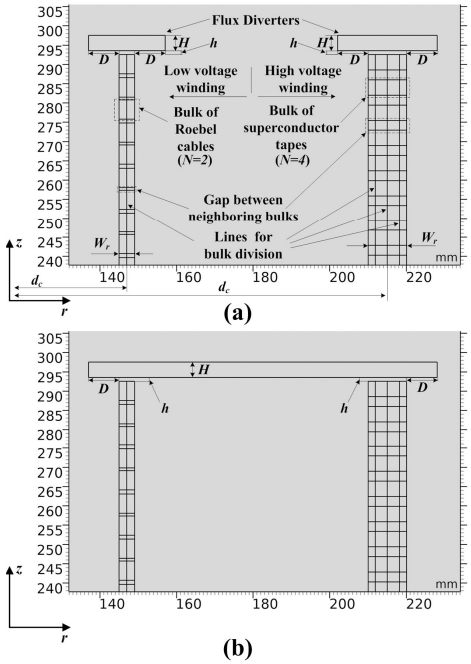

Fig. 2. The 2D axial symmetric structures of the designs used for analysis (only the tops of the windings are shown).

Two designs based on an axial symmetric transformer winding model [24] are provided in Fig. 1, in which four and two FDs are applied to the ends of the windings, respectively [16], [19]. Fig. 2 shows the 2D sections of the designs used for analysis in COMSOL Multiphysics. A 2D cylindrical coordinate (r, z) is used, where r and z axes indicate the radial and axial directions, respectively. The two vertical strips in Fig. 2 represent the LV and HV windings, respectively. The horizontal strips represent the FDs. The key parameters of the FDs, including an indication of width D, the height of the FDs H, the height of the gaps between the FDs and the windings h are used for evaluation. In the case of the four flux diverters, $2 \times D$ is the difference between the width of a flux diverter and the corresponding winding. When the two flux diverters are used, D is the difference between the inner radiuses of the FDs and the LV winding, and the difference between the outer radiuses of the FDs and the HV winding. The main parameters of the transformer windings are summarized in Table I.

TABLE I
PARAMETERS OF SUPERCONDUCTOR WINDINGS

Parameters	LV winding	HV winding
Total height [mm]	585	585
Inner radius [mm]	145	210
Outer radius [mm]	149	220
Turns (in r direction)	3	22
Turns (in z direction)	50	90
Nominal current I_n [A]	871.2	66
Tape critical current density at zero field (65 K) [A/mm]	114	114
Tape width [mm]	5	4
Tape thickness [mm]	0.12	0.12
Rated voltage [kV]	1.9	25

The LV winding is built in a solenoid structure, which uses 9/5 Roebel cables (9 intertwined tapes of width 5 mm) to provide large current [16]. The odd number 9 introduces uneven distribution, which can be modeled using a homogenization approach provided in Section II. Each Roebel cable is comprised of two sides with 4 and 5 tapes, respectively, and a gap in between. Thus, 3 turns of the Roebel cables in the radial direction are represented by 2 bulks and a gap between the bulks, as shown in Fig. 2b. There are 100 bulks (50 turns of the cables) along the axial direction. The HV winding is composed of double pancake coils (DPCs). Each pancake is modeled as a bulk with 22 turns of tapes. In total, 45 DPCs are used and represented by 90 bulks along the axial direction. To reduce the computation cost and maintain sufficient modeling accuracy [16], all the bulks are divided using $N-1$ lines perpendicular to the r axis at (L_r, 0)

$$L_r(i) = \frac{1}{2} * W_r * (\pm \frac{\log(i)}{\log(N)}) + d_c, \quad i = 1, 2, ..., N\text{-}1, \quad N \geq 2 \tag{1}$$

where N is the number of areas divided in a bulk of the LV winding or HV winding, W_r is the width of the bulk and d_c is the horizontal distance between the bulk center and the z axis. From Table I, the widths of the bulks in the LV and HV windings are 4 mm and 10 mm, and the distances d_c are 147 mm and 215 mm, respectively. Considering the widths of the LV and HV windings, $N = 2$ and $N = 4$ are used for the division, respectively.

B. Means of Evaluating AC losses and Magnetic Fields of the Designs

The strategic distribution of the lines obtained from (1) is used in the homogenization approach, such that when $N > 2$, regions closer to the vertical boundaries of the windings are divided into smaller areas, as suggested by the HV winding in Fig. 2. These regions are more likely to be penetrated by magnetic flux, hence modeling accuracy is required. This indicates that the homogenization is a time efficient approach with a minimal compromise of the accuracy. Uniformly distributed conductive materials are defined for homogenization of the superconductor tapes and insulation layers in the LV and HV windings respectively, which satisfy an $E-J$ relation.

$$\frac{E}{E_c} = (\frac{J}{J_{c.eng}})^n \tag{2}$$

where the critical electric field $E_c = 10^{-4}$ V/m, $n = 30$, $J_{c.eng}$ is the engineering critical current density inferred from [17]

$$J_{c.eng}(B) = \frac{N_t * S_t * J_{c0}}{S_b} * (1 + \frac{k^2 B_z^2 + B_r^2}{B_0^2})^{-\alpha} \tag{3}$$

where N_t is the number of turns in a bulk, which satisfies $N_t = 9 * 3/2 = 13.5$ on average for the LV winding as the 9/5 Roebel cable is used, and $N_t = 22$ for the HV winding. The areas of the turns within the LV and HV windings S_t are 0.6 mm^2 and 0.48 mm^2, respectively. The areas of the bulks within the LV and HV windings S_b are 20 mm^2 and 40 mm^2, respectively. The critical current density at zero field and 65 K is $J_{c0} = 114 \div 0.12 = 950$ A/mm^2. The areas of the gaps between the bulks are not used to infer $J_{c.eng}$, since they are modeled as part of the air domain that surrounds the windings. Three parameters, $k = 0.71$, $B_0 = 0.1$ T and $\alpha = 0.23$ are characteristics associated with magnetic field dependence of the materials [17], B_r and B_z can be obtained using (2) applied to the following Maxwell equations

$$J = \nabla \times H, \tag{4}$$

$$\nabla \times E = -\frac{\partial \mathrm{B}}{\partial \mathrm{t}}. \tag{5}$$

The 2D axial symmetric model is then analyzed using an H formulation [17]

$$\mu_0 \mu_r \frac{\partial H_r}{\partial t} - \frac{1}{r} \frac{\partial (r\rho(\frac{\partial H_r}{\partial z} - \frac{\partial H_z}{\partial r}))}{\partial \mathrm{z}} = 0, \tag{6}$$

$$\mu_0 \mu_r \frac{\partial H_z}{\partial t} + \frac{1}{r} \frac{\partial (r\rho(\frac{\partial H_r}{\partial z} - \frac{\partial H_z}{\partial r}))}{\partial r} = 0. \tag{7}$$

where μ_0 is the vacuum permeability, μ_r and ρ are the relative permeability and resistivity of the materials. Furthermore, pointwise constraints P_{c_LV} and P_{c_HV} are applied to the bulks in the LV and HV windings.

$$P_{c\_LV} = J_{eng} - \frac{\iint \boldsymbol{J} \mathrm{d}S}{\iint \mathrm{d}S}, \tag{8}$$

$$P_{c\_HV} = J_{eng} + \frac{\iint \boldsymbol{J} \mathrm{d}S}{\iint \mathrm{d}S} \tag{9}$$

where S is used for the area integration and J is inferred from (4). The engineering current density is obtained using

$$J_{eng} = \frac{N_t * I_n}{S_b} \tag{10}$$

where the nominal current I_n is provided in Table I. The AC loss P is

$$P = \iiint \mathrm{E} * J \mathrm{d}V. \tag{11}$$

where V is the volume of the bulks of the windings. The magnetic flux density B satisfies

$$|B| = \sqrt{B_r^2 + B_z^2} \tag{12}$$

where $|B|$ is used for evaluating the magnetic flux distribution.

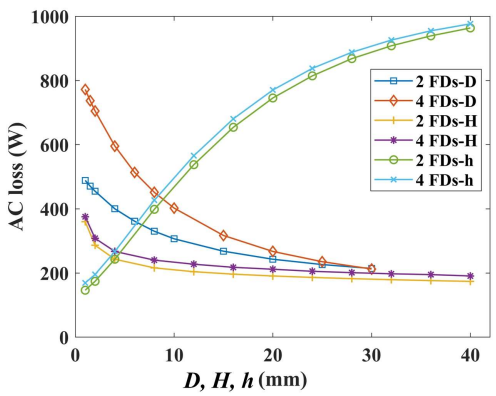

Fig. 3. The AC losses of the windings with the increased *D, H and h*.

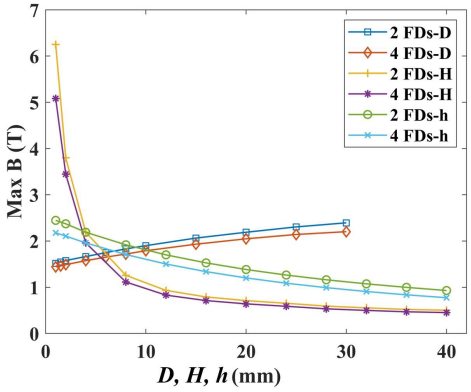

Fig. 4. The maximum magnetic flux densities of the windings with the increased *D, H and h*.

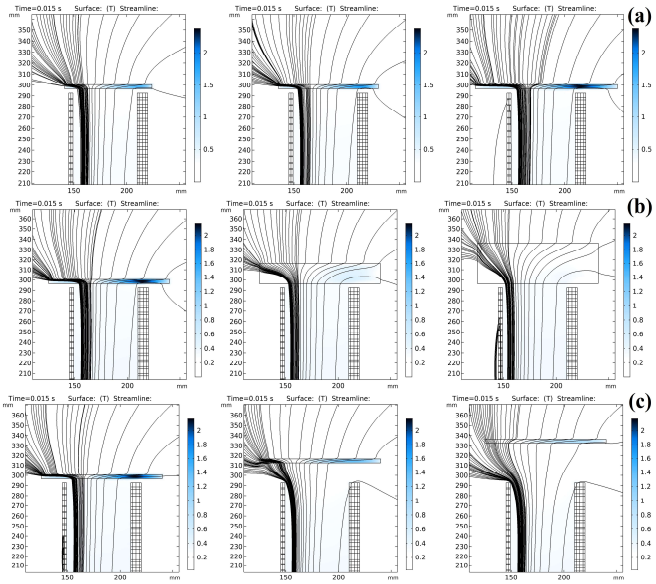

Fig. 5. The magnetic flux distributions of the 2 FDs model with (a) H = 4 mm, h = 4 mm, and D = 4, 10, 30 mm. (b) D = 20 mm, h = 4 mm, and H = 4, 20, 40 mm. (c) D = 20 mm, H = 4 mm, and h = 4, 20, 40 mm.

III. Analysis of the Two Designs

The HTS transformer winding model using parameters provided in Table I was first built and analyzed in [24]. In the case of no FDs applied to the windings, the AC loss is 1062.1 W. The magnetic flux intensively penetrates into the ends of the windings, which leads to considerable losses. The designs with the 4 and 2 flux diverters, namely the 4 FDs design and 2 FDs design are analyzed using COMSOL, respectively. To begin with, the widths of the FDs are increased for the AC loss and magnetic flux density analysis of the windings. Furthermore, the heights of the FDs and the gaps between the FDs and the windings are increased in turn for the analysis. The relative permeabilities of the FDs μ_r were assumed to be 100, 500, 1000 and 5000, and applied to a series of parameter combinations. For both designs, the variation of the relative permeabilities provided close results of AC losses and maximum magnetic flux densities with differences less than 0.5%. As consequences, only $\mu_r = 100$ is assigned to the FDs. The windings, including the bulks and gaps, and the air domain are assigned with $\mu_r = 1$.

A. The Influence of D on the AC Losses and Magnetic Flux Densities

The two designs are applied with $H = 4$ mm, $h = 4$ mm and D is increased from 1 mm to 30 mm. If D is further increased in the case of the 4 FDs, the FDs of the LV and HV windings will be overlapped, thus 30 mm is chosen as the maximum. The AC losses are reduced significantly from 772.2 W to 212.4 W, and from 488.6 W to 214.2 W respectively, as shown by the 4FDs-D and 2FDs-D in Fig. 3. The increased D leads to the reduction of the AC losses in the two cases. Furthermore, the 2 FDs design has shown better results in most cases. This indicates that wider FDs are more capable of reducing AC losses. However, in the case of $D = 30$ mm, the 4 FDs design has a slightly better performance. As the relative tolerance and absolute tolerance of the designs are set as 10^{-4} and 10^{-5}, respectively, 212.4 W and 214.2 W may not simply be considered as close results. The 4 FDs design achieves lower AC losses if the widths of the FDs are sufficiently large. Note that the increased D leads to a less effective AC loss reduction. Thus, H and h should also be adjusted for designing high efficiency FDs.

The magnetic flux densities of the designs $|B|$ are obtained and the maximum value is shown by the 4FDs-D and 2FDs-D in Fig. 4. The maximum densities of the two designs are increased from 1.4 T to 2.2 T, and from 1.5 T to 2.4 T, respectively. In the both cases, the wider FDs lead to the increased magnetic flux densities. Furthermore, the 4 FDs design can be a better solution for reducing the magnetic flux densities.

B. The Influence of H on the AC Losses and Magnetic Flux Densities

The two designs are applied with $D = 20$ mm, $h = 4$ mm and H is increased from 1 mm to 40 mm. As suggested from the 4FDs-H and 2FDs-H in Fig. 3, the AC losses are reduced significantly from 375.5 W to 190.8 W and from 359.8 W to 173.9 W, respectively. The increased H leads to AC loss reduction in the two cases. Meanwhile, this also leads to less effective AC loss reduction. In Fig. 4, the 4FDs-H and 2FDs-H show that the maximum magnetic flux densities are reduced from 5.1 T to 0.5 T (approximation of 0.45 T), and from 6.2 T to 0.5 T (approximation of 0.50 T), respectively. This indicates that the 4 FDs design has comparatively lower magnetic flux densities.

C. The Influence of h on the AC Losses and Magnetic Flux Densities

The two designs are applied with $D = 20$ mm, $H = 4$ mm and h is increased from 1 mm to 40 mm. As suggested from the 4FDs-h and 2FDs-h in Fig. 3, the AC losses are increased from 169.0 W to 976.5 W, and from 146.31 W to 963.61 W, respectively. The increased h leads to the higher AC losses in the two cases. Meanwhile, the 2 FDs design has lower AC losses compared with the 4 FDs design. In Fig. 4, the 4FDs-h and 2FDs-h show that the maximum magnetic flux densities are reduced from 2.2 T to 0.8 T, and from 2.4 T to 0.9 T, respectively. This suggests that the 4 FDs design has comparatively lower magnetic flux densities.

D. Magnetic Flux Distributions of the 2 FDs Design

Fig. 5 shows the magnetic flux distributions of the 2 FDs design, where the magnetic flux is obtained from (B_r, B_z) as results of the H formulation, and the magnetic flux densities are obtained using (10). The flux lines are more intensive in regions close to the LV winding due to the large current, which can be explained using (4). Meanwhile, the maximum |B| are observed in the flux diverters and the regions are close to the HV winding. This suggests high voltages of the HTS windings lead to high magnetic flux densities of the flux diverters. In Fig. 5a where $H = 4$ mm, $h = 4$ mm, and $D = 4$, 10, 30 mm, it can be seen that the FDs with the increased D are more effective in diverting flux due to the larger volume. In Fig. 5b where $D = 20$ mm, $h = 4$ mm, and $H = 4$, 20, 40 mm, the FDs with the increased H are also more effective due to this reason. In Fig. 5c where $D = 20$ mm, $H = 4$ mm, and $h = 4$, 20, 40 mm, it can be seen that the decreased h leads to less flux penetration at the ends of the windings.

IV. Conclusion

A 1.65 MVA HTS transformer winding model was developed for AC loss and magnetic flux density analysis. Two designs of flux diverters were considered for AC loss reduction and magnetic flux optimization. The results indicate that the increased widths of the flux diverters result in lower AC losses but higher maximum magnetic flux densities. The increased heights of the flux diverters decrease both AC losses and maximum magnetic flux densities. The increased spatial distances between the flux diverters and the windings result in higher AC losses and lower maximum magnetic flux densities.

The increase of widths and heights of flux diverters, and decrease of spatial distances between the flux diverters and the windings are reasonable considerations for developing winding models with high efficiency. However in real practices, the parameters should also meet requirements of spatial and maximum magnetic flux density constraints. The proposed designs provide an effective and flexible means for designing or evaluation of transformer windings. The optimization of the structures of the flux diverters, and evaluation of the designs under different applied currents can be considered in the future.

REFERENCES

[1] J. X. Jin *et al*., "HTS Power Devices and Systems: Principles, Characteristics, Performance, and Efficiency," *IEEE Trans. Appl. Superconduct.*, vol. 26, no. 7, Oct. 2016, Art no. 3800526.

[2] Y. D. Chung, C. Y. Lee, H. K. Kang and Y. G. Park, "Design Consideration and Efficiency Comparison of Wireless Power Transfer With HTS and Cooled Copper Antennas for Electric Vehicle," *IEEE Trans. Appl. Superconduct.*, vol. 25, no. 3, June 2015, Art no. 5000205.

[3] G. Bai, C. Gu and L. Lai, "Electromagnetic Analysis of an Air-Core HTS Transformer," *IEEE Trans. Appl. Superconduct.*, vol. 29, no. 2, Mar. 2019, Art no. 5501003.

[4] H. Lee, C. Jung, C. S. Song, S. Lee, B. Yang and G. Jang, "Novel Protection Scheme With the Superconducting Power Cables and Fault Current Limiters Through RTDS Test in Icheon Substation," *IEEE Trans. Appl. Superconduct.*, vol. 22, no. 3, June 2012, Art no. 4705304.

[5] Z. Deng, L. Wang, H. Li, J. Li, H. Wang and J. Yu, "Dynamic Studies of the HTS Maglev Transit System," *IEEE Trans. Appl. Superconduct.*, vol. 31, no. 5, Aug. 2021, Art no. 3600805.

[6] W. Song, X. Pei, J. Xi and X. Zeng, "A Novel Helical Superconducting Fault Current Limiter for Electric Propulsion Aircraft," *IEEE Trans. Transp. Electrification*, vol. 7, no. 1, pp. 276-286, Mar. 2021.

[7] Y. Asrami, M. Staines and M. Sidorov, "Fault current limiting HTS transformer with extended fault withstand time," *Supercond. Sci. Technol.*, vol. 32, no. 3, Jan. 2019, Art no. 035006.

[8] D. Hu *et al*., "Characteristic Tests and Electromagnetic Analysis of an HTS Partial Core Transformer," *IEEE Trans. Appl. Superconduct.*, vol. 26, no. 4, June 2016, Art no. 5500305.

[9] Xiaosong Li, Qiaofu Chen, Gui Hu, Jianbo Sun and Guzong Long, "Numerical analysis on magnetic field of HTS transformer with different geometry," *IEEE Trans. Magn.*, vol. 42, no. 4, pp. 1343-1346, Apr. 2006.

[10] F. Irannezhad and H. Heydari, "Conducting a Survey of Research on High Temperature Superconducting Transformers," *IEEE Trans. Appl. Superconduct.*, vol. 30, no. 6, Sept. 2020, Art no. 5500613.

[11] M. Yazdani-Asrami, M. Staines, G. Sidorov, and A. Eicher, "Heat transfer and recovery performance enhancement of metal and superconducting tapes under high current pulses for improving fault current-limiting behavior of HTS transformers," *Supercond. Sci. Technol.*, vol. 33, no. 9, Aug. 2020, Art no. 095014.

[12] Z. Jiang, W. Song, X. Pei, J. Fang, R. A. Badcock, and S.C. Wimbush, "15% reduction in AC loss of a 3-phase 1 MVA HTS transformer by exploiting asymmetric conductor critical current," *J. Phys. Commun.*, vol. 5, no.2, Feb. 2021, Art no. 025003.

[13] J. Kvitkovic, M. Polak and P. Mozola, "Distribution of Magnetic Field Inside the Winding of a BSCCO Coil," *IEEE Trans. Appl. Superconduct.*, vol. 18, no. 2, pp. 1621-1624, June 2008.

[14] Y. Q. Xing *et al*., "Influence of Flux Diverter on Magnetic Field Distribution for HTS Transformer Windings," *IEEE Trans. Appl. Superconduct.*, vol. 26, no. 7, Oct. 2016, Art no. 5501305.

[15] M. Polak, E. Pardo, P. Mozola and J. Souc, "Magnetic Field in the Winding of an YBCO Pancake Coil: Experiments and Calculations," *IEEE Trans. Appl. Superconduct.*, vol. 22, no. 3, June 2012, Art no. 6600204.

[16] W. Song, Z. Jiang, X. Zhang, M. Staines, R. Badcock, J. Fang, Y. Sogabe, and N. Amemiya, "AC loss simulation in a HTS 3-Phase 1 MVA transformer using H formulation," *Cryogenics*, vol. 94, pp. 14-21, 2018.

[17] W. Song, Z. Jiang, M. Staines, S. Wimbush, R. Badcock and J. Fang, "AC Loss Calculation on a 6.5 MVA/25 kV HTS Traction Transformer With Hybrid Winding Structure," *IEEE Trans. Appl. Superconduct.*, vol. 30, no. 4, June 2020, Art no. 5500405.

[18] S. Wu, J. Fang, L. Fang, A. Zhang, Y. Wang and Y. Wu, "The Influence of Flux Diverter Structures on the AC Loss of HTS Transformer Windings," *IEEE Trans. Appl. Superconduct.*, vol. 29, no. 2, Mar. 2019, Art no. 5501105.

[19] A. Moradnouri, M. Vakilian, A. Hekmati and M. Fardmanesh, "Optimal Design of Flux Diverter Using Genetic Algorithm for Axial Short Circuit Force Reduction in HTS Transformers," *IEEE Trans. Appl. Superconduct.*, vol. 30, no. 1, Jan. 2020, Art no. 5500108.

[20] M. D. Ainslie, D. Hu, J. Zou and D. A. Cardwell, "Simulating the In-Field AC and DC Performance of High-Temperature Superconducting Coils," *IEEE Trans. Appl. Superconduct.*, vol. 25, no. 3, June 2015, Art no. 4602305.

[21] A. Moradnouri, M. Vakilian, A. Hekmati and M. Fardmanesh, "The Impact of Multilayered Flux Diverters on Critical Current in HTS Transformer Windings," *Proc. Iran. Conf. Electr. Engr.*, 2019, pp. 481-485.

[22] M. K. Al-Mosawi, K. Goddard, C. Beduz and Y. Yang, "Coreless HTS Synchronous Generator Operating at Liquid Nitrogen Temperatures," *IEEE Trans. Appl. Superconduct.*, vol. 17, no. 2, pp. 1599-1602, June 2007.

[23] Y. Chen, X. Y. Chen, L. Zeng, Q. Xie and Y. Lei, "AC Loss and Temperature Simulations of HTS Pancake Coil during SMES Operations," *Proc. IEEE Int. Conf. Appl. Superconduct. Electromagn. Devices*, 2020.

[24] X. Fang, X. Wang, W. Liu, J. Fang, W. Song and X. Pei, "Magnetic Field and AC Loss Analysis of 2G HTS Transformer Windings Applied with Flux Diverters," *Proc. IEEE Int. Conf. Appl. Superconduct. Electromagn. Devices*, 2020.

[25] Z. Li, Z. Li, H. Li, Z. Wang and X. Di, "The Influence of Flux Diverters on AC Loss of Single Pancake Coil Used in HTSPPT," *Proc. IEEE Int. Conf. Appl. Superconduct. Electromagn. Devices*, 2020.